Supporting Information

Ultrafast Energy Transfer from Polymer Donors Facilitating Spectral Uniform Photocurrent Generation and Low Energy Loss in High-efficiency Nonfullerene Organic Solar Cells

Zeng Chen[1,2], Chengliang He[3], Peng Ran[4], Xu Chen[4], Yao Zhang[1], Chi Zhang[1], Runchen Lai[4], Yang (Michael) Yang[4], Hongzheng Chen[3], Haiming Zhu[1,2]*

[1]State Key Laboratory of Modern Optical Instrumentation, Key Laboratory of Excited State Materials of Zhejiang Province, Department of Chemistry, Zhejiang University, Hangzhou, Zhejiang 310027, China.

[2]ZJU Hangzhou Global Scientific and Technological Innovation Center, Hangzhou, Zhejiang 311200, China.

[3]State Key Laboratory of Silicon Materials, MOE Key Laboratory of Macromolecular Synthesis and Functionalization, International Research Center for X Polymers, Department of Polymer Science and Engineering, Zhejiang University, Hangzhou 310027, P. R. China.

[4]State Key Laboratory of Modern Optical Instrumentation, Key Laboratory of Excited State Materials of Zhejiang Province, College of Optical Science and Engineering, Zhejiang University, Hangzhou, Zhejiang 310027, China.

* Corresponding author: hmzhu@zju.edu.cn

Supplemental Experimental Procedures

Materials   Poly[(2,6-(4,8-bis(5-(2-ethylhexyl-3-fluoro)thiophen-2-yl)-benzo][1,2-b:4,5-b']dithiophene))-alt-(5,5-(1',3'-di-2-thienyl-5',7'-bis(2-ethylhexyl)benzo[1',2'-c:4',5' -c']dithiophene-4,8-dione) (PM6), Y6 and CH1007 were purchased from Solarmer Energy Inc (Beijing, China). L8-BO was purchased from Guangzhou ChasingLight Technology Co LTD (Guangzhou, China). IXIC-4Cl was purchased from Derthon Optoelectronic Materials Science Technology Co LTD (Shenzhen, China). BTP-S2 and BTPV-4F were synthesized as previous reported [1, 2]. All materials were used as received without additional purification. The pre-patterned indium-tin oxide (ITO)-coated glass substrates were purchased from South China Xiang Science & Technology Company Limited (China) with a sheet resistance of 15 Ω sq^{-1}.

Film/Devices Fabrication

Organic solar cells were fabricated on glass substrates commercially pre-coated with a layer of ITO, based on the inverted structure: ITO/PEDOT:PSS/Active Layer/PFN-Br/Ag. Before fabrication, the substrates were consecutively pre-cleaned by an ultrasonic bath of detergent, deionized water, acetone, and isopropanol, and then treated in an ultraviolet ozone generator for 15 min. Then, a thin PEDOT:PSS (Baytron P AI4083) layer was spin coated onto the substrates at 4500 rpm for 30 s and annealed at 170 °C for 20 min. The substrates were placed into a glovebox and all active layers were spin coated from (PM6: acceptor = 1:1.2) chloroform solution (see Note S6 for details about the preparation of BHJ films and neat films). Then, a ~5 nm PFN-Br film was deposited as the cathode buffer layer by spin-coating at 4000 rpm for 30 s from a solution of 0.5 mg/mL PFN-Br in methanol. Finally, the Ag (80 nm) electrode was deposited by thermal evaporation under high vacuum (<3×10^{-4} Pa) to complete the device

fabrication.

Film and device characterization The absorption spectrum was measured by Agilient Carry 7000 UV-Vis spectrometer. Steady-state PL were detected using a home-setup microfluorescence system. The excitation light (532nm and 785nm) was generated by a CW laser. The emission light was collected using a spectrograph (Princeton Instruments, Acton SpectraPro, SP-2300i) with a 800 mm^{-1} grating and detected by a liquid-N_2-cooled CCD (PyLon 100B excelon). Cyclic voltammetry (CV) was done on a CHI600A electrochemical workstation with Pt disk, Pt plate, and standard calomel electrode (SCE) as working electrode, counter electrode, and reference electrode, respectively, in a 0.1 mol/L tetrabutylammonium hexafluorophosphate (Bu_4NPF_6) CH_2Cl_2 solution. The CV curves were recorded versus the potential of SCE, which was calibrated by the ferrocene-ferrocenium (Fc/Fc+) redox couple (4.8 eV below the vacuum level). Current density−voltage (J−V) characteristics were measured under AM1.5G light (1000 W/m^2) with the xenon arc lamp of a Class A solar simulator. Light intensity was calibrated by a Newport-calibrated mono crystalline Si diode. The Keithley 2400 source meter was used for I-V measurement. External quantum efficiency (EQE) was characterized by PT-QEM 1000 with a standard silicon solar cell as correction. The I-V and EQE tests were carried out in a glove box filled with N2 and the devices were unencapsulated. Atomic force microscopy (AFM) images were taken on a Cypher S Atomic Force Microscope.

Transient absorption spectroscopy For femtosecond transient absorption spectroscopy, the fundamental output from Yb:KGW laser (1030 nm, 220 fs Gaussian fit, 100 kHz, Light Conversion Ltd) was separated to two light beams. One was introduced to NOPA (ORPHEUS-N, Light Conversion Ltd)

to produce a certain wavelength as the pump beam (here we use 550 nm, 750 nm, below 5 μJ/cm^2 and higher power pulse, 30 fs pulse duration), the other was focused onto a YAG plate to generate white light continuum as the probe beam. The pump and probe beams overlapped on the sample at a small angle less than 10°. The transmitted probe light from sample was collected by a linear CCD array and a liquid-N$_2$-cooled CCD (PrLoN-IR). The transmitted probe light with (T_{pump}) and without (T_{unpump}) pump were collected and the normalized transmittance change $\Delta T/T$ was calculated by $\Delta T/T = (T_{pump} - T_{unpump})/T_{unpump}$. The films used for TA measurements were loaded in a chamber filled with N2 with four closed transparent windows, preventing some other excited state processes like photooxidation. Limited by the measurement factors that we can just measure the power density without the chamber, the real excitation power will be smaller than the value we measured.

Femtosecond time-resolved photoluminescence (fs-TRPL) Femtosecond PL emission experiments use the same laser source as the TA measurements. The original 1030-nm femtosecond laser was used as the gate beam, and fs laser of 550 nm and 750 nm were used as the pump beams. The delay between the pump and probe pulses was controlled by a motorized delay stage. Emission from the samples was collected after a 900 nm long pass filter and a 950 nm short pass filter focused onto a 1-mm BBO crystal together with the gate beam to generate a sumfrequency signal. The sum-frequency signal was focused into a fibercoupled monochrometer and detected by a photomultiplier tube (PMT).

Electroluminescence Quantum Efficiency (EQE$_{EL}$) measurements The value of EQE$_{EL}$ were detected with a home-built system using a spectrograph (Princeton Instruments) with a liquid-N2-cooled CCD (PrLoN-IR) at -100 °C. A Keithley 2614B meter connected with devices was used to supply voltages and record the injected current. The devices used for EQE$_{EL}$ measurements were encapsulated before exposing
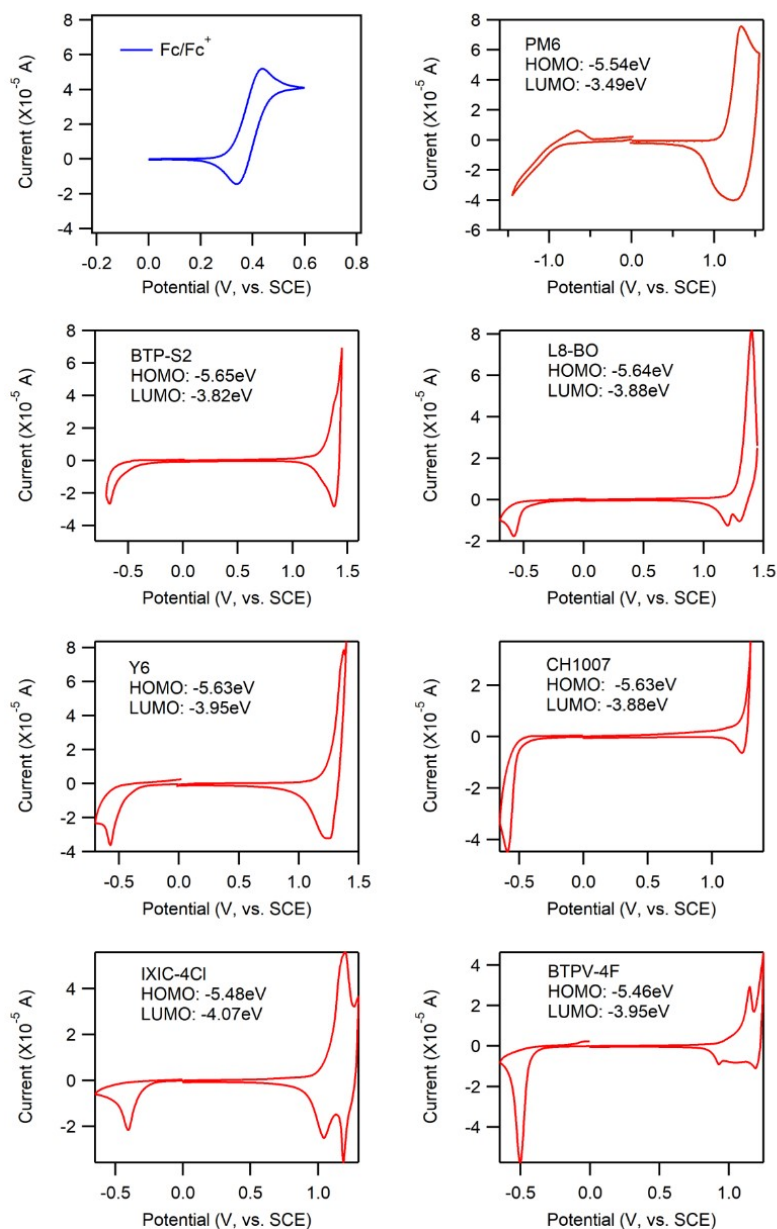
to air.

Supplemental Figures and Notes

Figure S1. Cyclic voltammograms and the energy levels of PM6, BTP-S2, L8-BO, Y6, CH1007, IXIC-4Cl, BTPV-4F and Fc/Fc$^+$.

Note: Cyclic voltammetry was done on a CHI600A electrochemical workstation by utilizing the acetonitrile solution of 0.1 mol/L tetrabutylammoniumhexafluorophosphate (Bu4NPF6). The CV curves were recorded versus the potential of SCE, which was calibrated by the ferrocene-ferrocenium (Fc/Fc$^+$)

redox couple (4.8 eV below the vacuum level). Then LUMO and HOMO levels was calculated by the equation of $E_{\text{LUMO/HOMO}} = -e\,(E_{red/ox}+4.41)$ (eV).
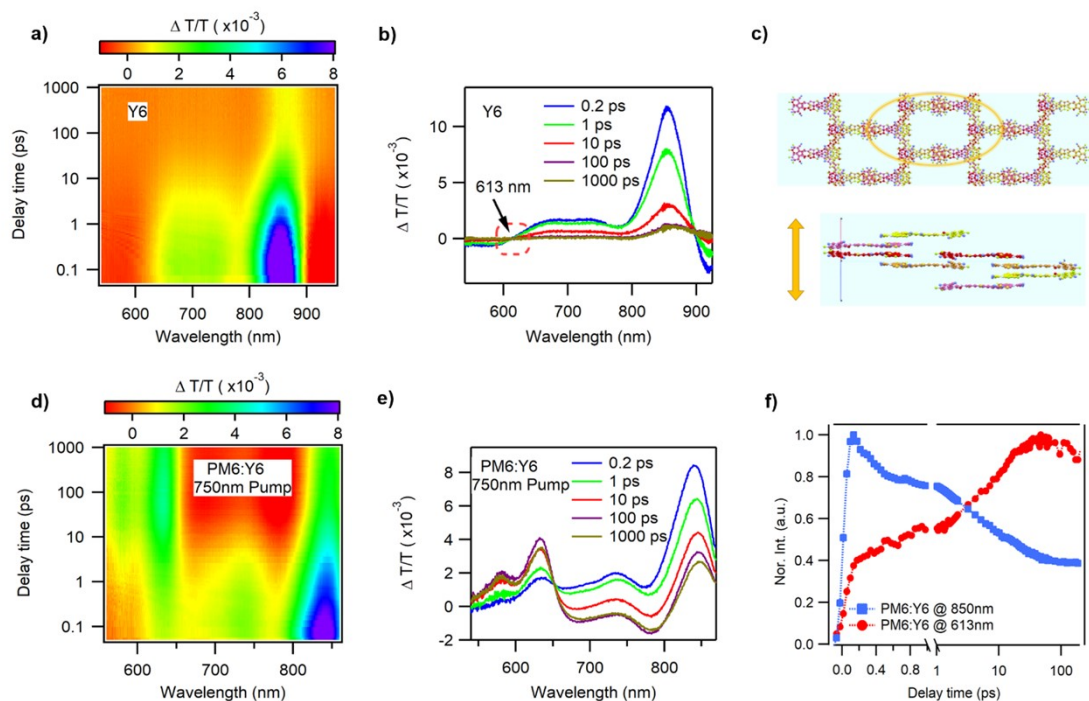

Figure S2. Hole transfer TA spectra and kinetics. (a) 2D color plot and (b) representative TA spectra at indicated delay times of neat Y6 film in visible area under 750 nm excitation at < 5 μJ/cm^2, showing no Y6 signal at ~613 nm. (c) Molecular stacking patterns of typical NFA(Y6) in the single-crystal structure. (d) 2D color plot and (e) representative TA spectra at indicated delay times of neat Y6 film in visible area under 750 nm excitation at <5 μJ/cm^2. (f) TA kinetics at 613 nm (red) and 850 nm (blue) for PM6: Y6 blend film under 750. The rise at 613nm and the decay at 850 nm represented the hole transfer process from Y6 to PM6.
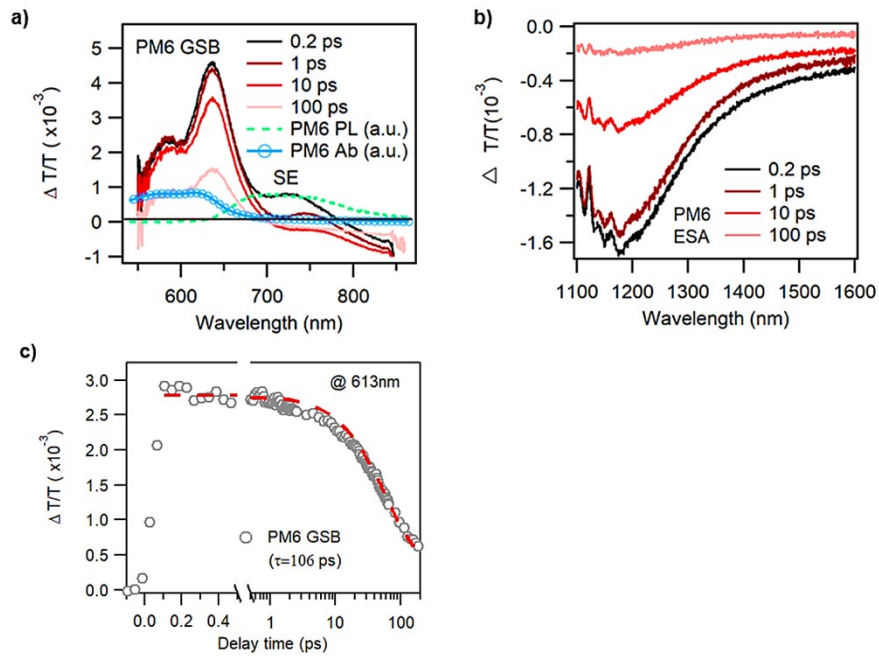
Figure S3. TA spectra evolution and kinetics of neat PM6 film. Representative fs-ps TA spectra at indicated early delay times of neat PM6 film in (a) visible and (b) NIR area under 550 nm excitation at < 5 μJ/cm^2. (c) The PM6 GSB decay at 613 nm and the lifetime with single exponential fit.
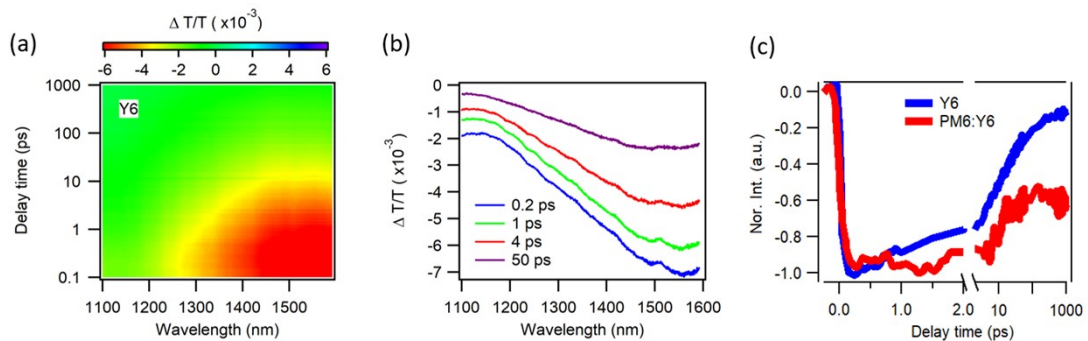
Figure S4. (a) 2D TA Color plot and (b) representative fs-ps TA spectra at indicated early delay times of neat Y6 film in NIR area under 750 nm excitation at < 5 μJ/cm^2. (c) Comparison of Y6 ESA kinetics at ~1550 nm recorded from neat Y6 film and PM6:Y6 blend film under 550 nm excitation.
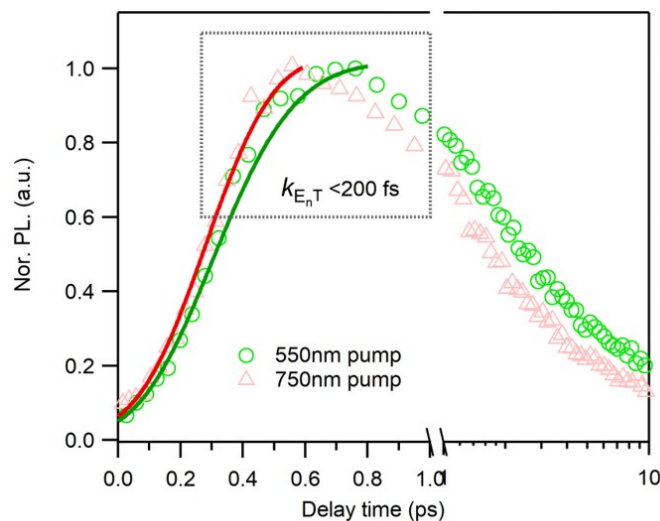

Figure S5. Femtosecond time-resolved photoluminescence (fs-TRPL) kinetics of Y6 emission in PM6:Y6 film under the excitation of 550 nm and 750 nm.
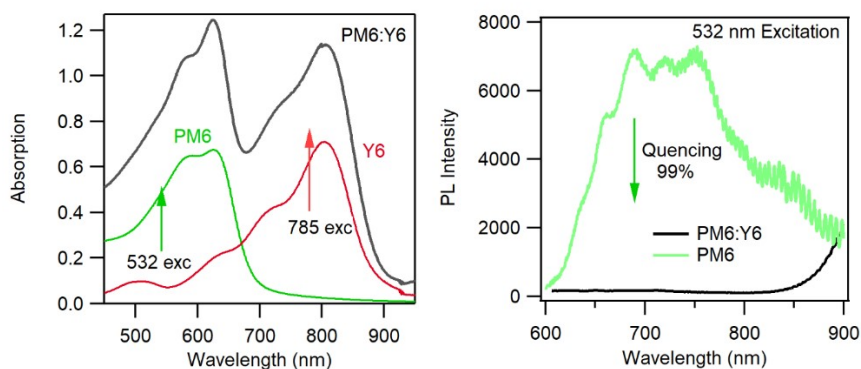
Figure S6. the absorption and PL results of PM6 and PM6: Y6.

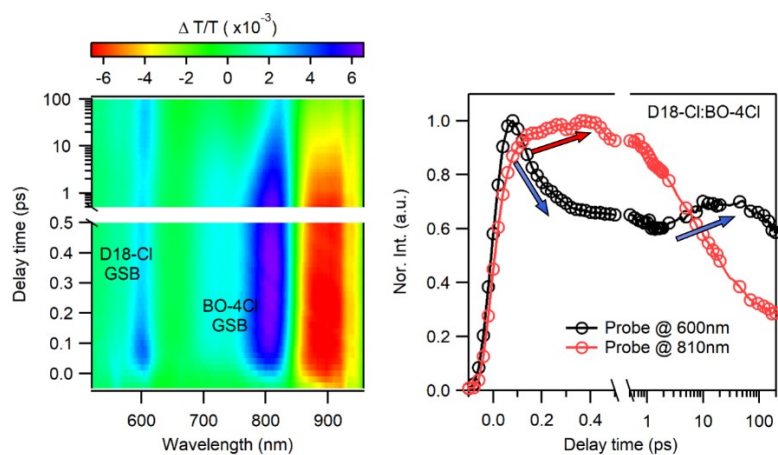Figure S7. 2D TA Color plot of D18-Cl:BO-4Cl blend film and corresponding GSB kinetics of donor D18-Cl (600 nm) and BO-4Cl (810 nm) under 550 nm excitation at < 5 $\mu J/cm^2$.

PM6:BTP-S2

PM6:L8-BO

PM6:Y6

PM6:CH1007

PM6:BTPV-4F

PM6:IXIC-4Cl

RMS:0.82 nm

RMS:0.81 nm

RMS:1.04nm

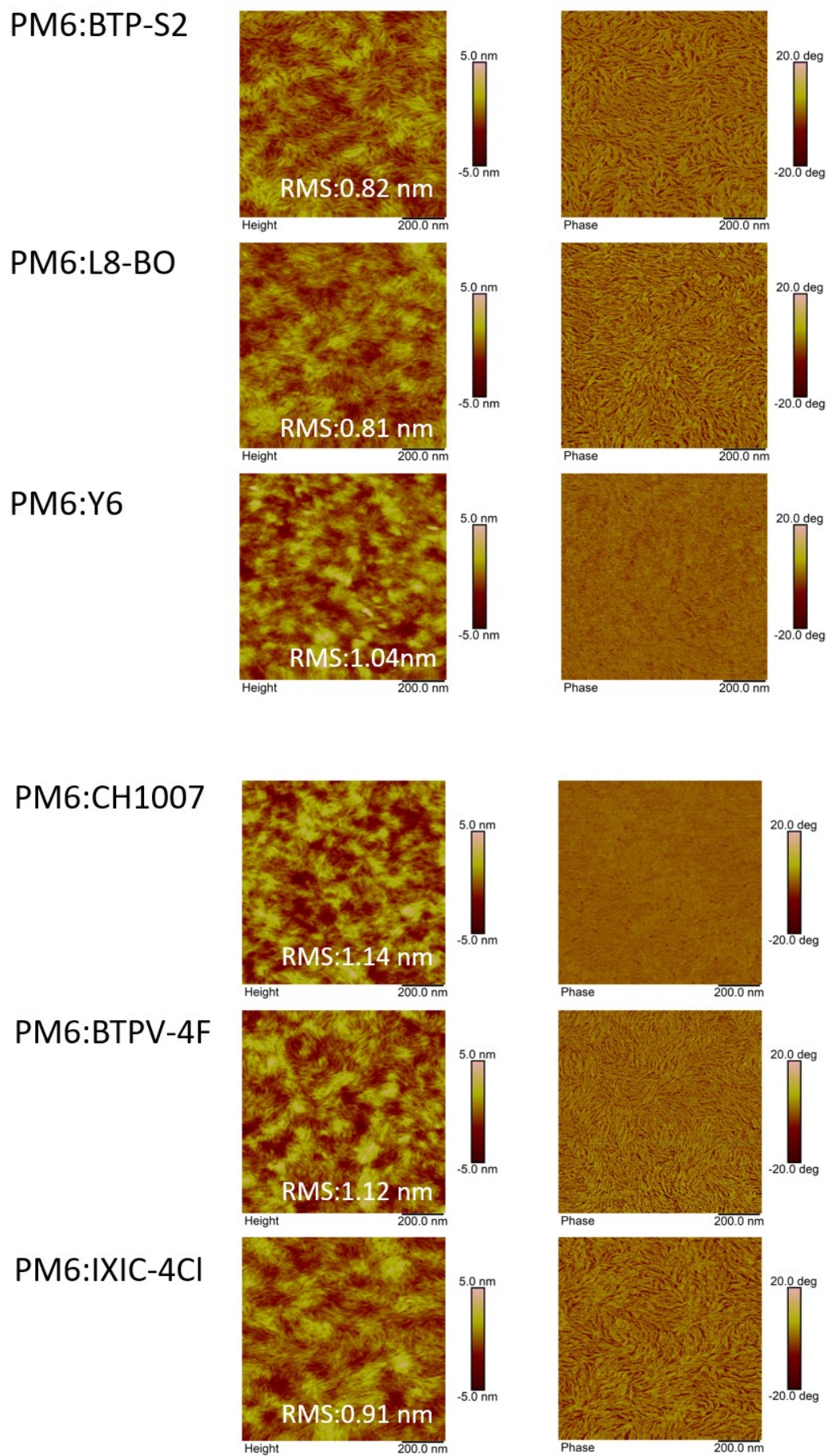RMS:1.14 nm

RMS:1.12 nm

RMS:0.91 nm

Figure S8. AFM images for PM6:NFAs blend films (Left: height image; Right: phase images).

Note S1

To reveal the role of energy transfer in blend, according to the optical absorption and photoluminescence (PL) results, we calculated the Förster resonance energy transfer efficiency based on the following equitation:

For neat NFA film,

$$\frac{S_{NFA(785EXC)}}{S_{NFA(532EXC)}} = \frac{I_{(785EXC)}\,\alpha_{NFA(785EXC)}\,QY_{NFA}}{I_{(532EXC)}\,\alpha_{NFA(532EXC)}\,QY_{NFA}}$$

For the blend,

$$\frac{S_{BHJ(785EXC)}}{S_{BHJ(532EXC)}} = \frac{I_{(785EXC)}\,\alpha_{BHJ(785EXC)}\,QY_{BHJ}}{I_{(532EXC)}\,\alpha_{BHJ(532EXC)}\,(P_A + (1 - P_A)\eta)\,QY_{BHJ}}$$

where S_{NFA} and S_{BHJ} represent the integral of PL intensity under different excitation conditions of neat NFAs and blend film, respectively. I represent the excitation power density. α is the absorbance at the corresponding wavelength. QY represent the fluorescence quantum yield. P_A is the absorption proportion of acceptor in blend at the wavelength of 532 nm, which can be acquired from the neat NFA and blend absorption spectra. η is the energy transfer efficiency from donor to acceptor. Combining equation (1) and (2), we conclude that

$$\eta = \frac{Q - P_A}{1 - P_A}$$

with

$$Q = \frac{S_{BHJ(532EXC)}S_{NFA(785EXC)}\alpha_{BHJ(785EXC)}\alpha_{NFA(532EXC)}}{S_{BHJ(785EXC)}S_{NFA(532EXC)}\alpha_{BHJ(532EXC)}\alpha_{NFA(785EXC)}}$$

To make this equation more clear, we assume $Q_{532=}\dfrac{S_{BHJ(532EXC)}}{S_{NFA(532EXC)}}$, $Q_{785=}\dfrac{S_{BHJ(785EXC)}}{S_{NFA(532EXC)}}$, $\alpha_{BHJ=}\dfrac{\alpha_{BHJ(785EXC)}}{\alpha_{BHJ(532EXC)}}$ and $\alpha_{NFA=}\dfrac{\alpha_{NFA(785EXC)}}{\alpha_{NFA(532EXC)}}$.

Therefore, $Q = \left(\dfrac{Q_{532}}{Q_{785}}\right)\left(\dfrac{\alpha_{BHJ}}{\alpha_{NFA}}\right)$

Here, the absorption spectra are shown in Figure S9, in addition to the PL results displayed in Figure S10.

The detail relative parameters and the energy transfer efficiency were summarized in Table S1.
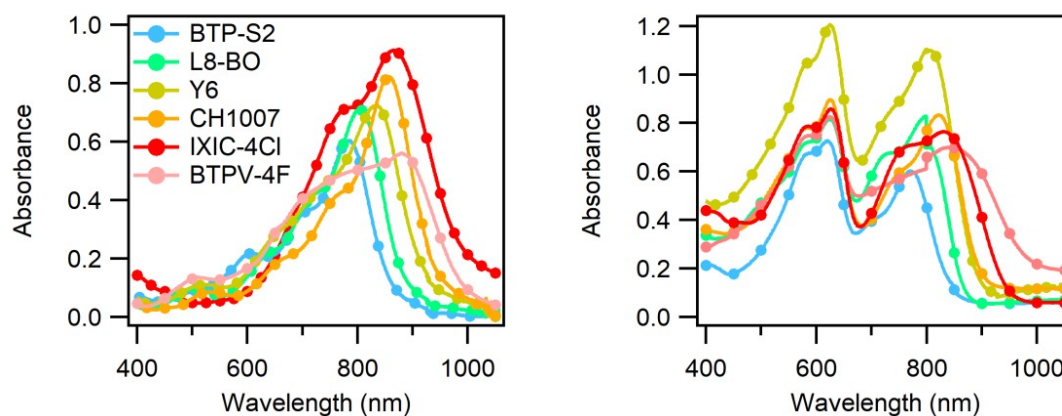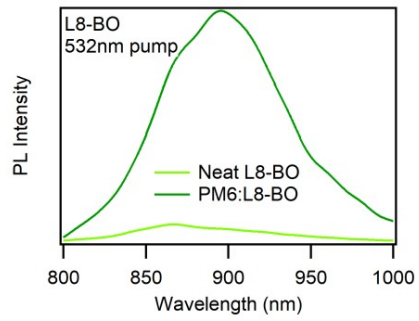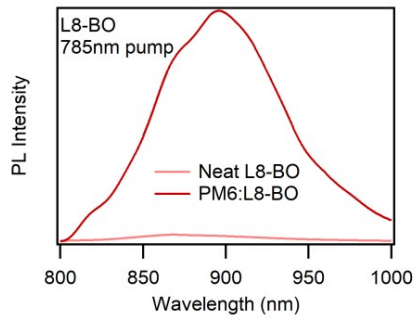

Figure S9. Absorbance spectra of neat NFAs films (left) and PM6: NFAs films (right).
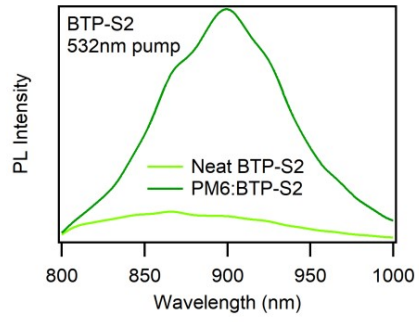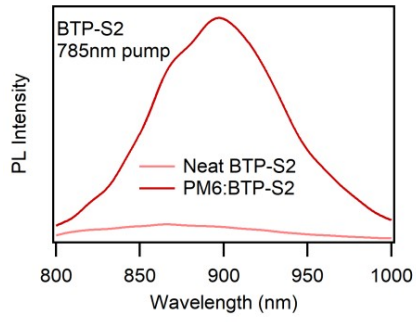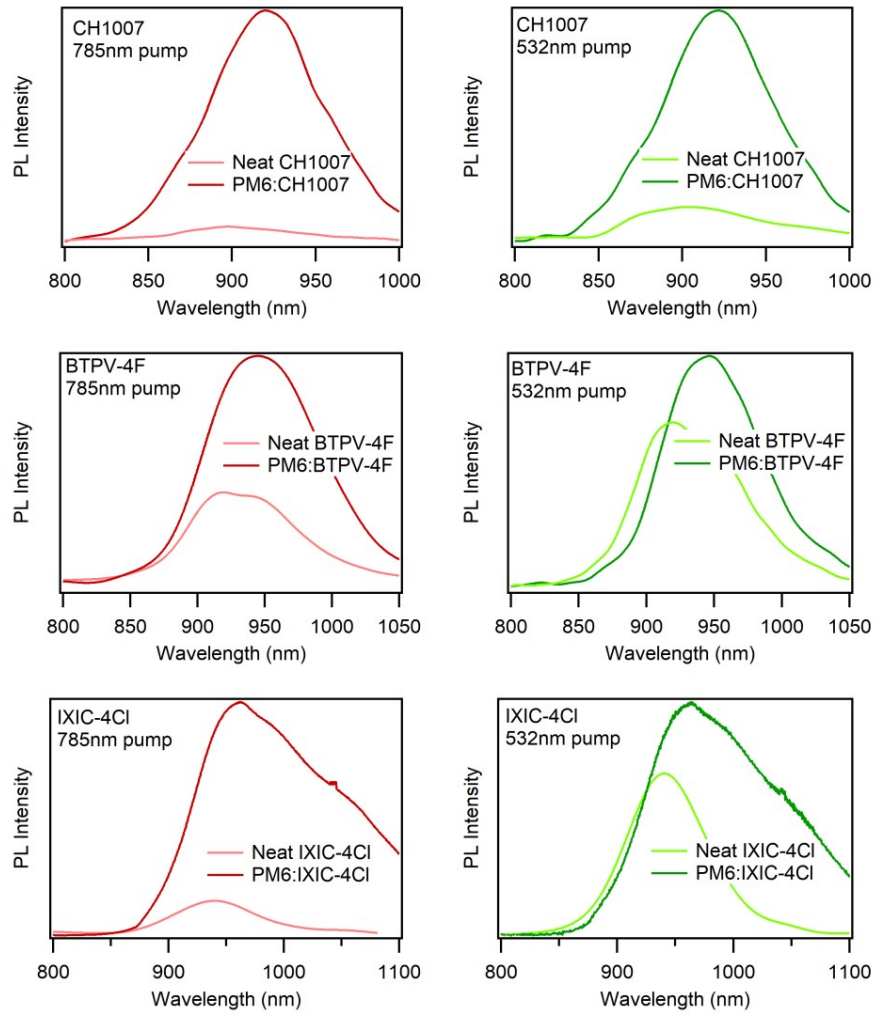
Figure S10. Steady-state photoluminescence (PL) spectra of the neat NFAs and PM6: NFAs films under the CW laser pump at 785 nm (left) and 532 nm (right).

Table S1. Detail parameters of energy transfer efficiency on PM6: NFAs films.

Sample	Q_{532}	Q_{785}	α_{BHJ}	α_{NFA}	Q	P_A	η
PM6: BTP-S2	0.121	0.069	1.00	3.52	0.500	0.282	0.303
PM6: L8-BO	0.075	0.028	1.15	4.34	0.710	0.249	0.611
PM6: Y6	0.108	0.044	1.09	4.56	0.587	0.218	0.473
PM6: CH1007	0.124	0.058	1.05	3.57	0.629	0.249	0.506
PM6: IXIC-4Cl	0.698	0.147	1.12	7.43	0.716	0.167	0.659

| PM6: BTPV-4F | 0.716 | 0.391 | 1.04 | 2.65 | 0.719 | 0.322 | 0.585 |

Note S2

Förster Resonance Energy Transfer (FRET) radius (r_0) is generally determined from the spectra overlap between the emission of donor and the absorption of acceptor as the following equation[3] :

$$r_0{}^6 = \left(\frac{9000 ln(10)}{128\pi^5 N_A}\right)\kappa^2 \emptyset_{PL}\left(\frac{\int_0^\infty F_D(\lambda)\varepsilon_A(\lambda)\lambda^4 d\lambda}{n(\lambda)^4}\right)$$

Where N_A is the Avogadro constant, κ^2 is the statistical orientation factor of the dipoles of donor relative to those of the acceptor, with the value of $\frac{2}{3}$ in the case of anisotropic donor/acceptor random distribution, $\emptyset_{PL}$ is the fluorescence quantum yield of neat donor, $F_D(\lambda)$ is the normalized fluorescence intensity of donor ($that\ is\ \int_0^\infty F_D\left(\frac{1}{\lambda}\right)d\left(\frac{1}{\lambda}\right) = 1$), and $\varepsilon_A(\lambda)$ is the molar extinction coefficient of acceptor along with the wavelength (λ), n is the refractive index.

Here, we calculate the relative overlap integral (J) by the following equation

$$J = \frac{\int_0^\infty F_D(\lambda)\varepsilon_A(\lambda)\lambda^4 d\lambda}{n(\lambda)^4}$$

Where $\varepsilon_A(\lambda)$ and $n(\lambda)$ were displayed in Figure S11, with $n(\lambda)$ can be calculated from the absorption and reflection spectra according to the n-k relation.[4] The value of J were listed in Table S2 for different nonfullerene acceptors based systems. So, we can simplify the value of r_0 as

$$r_0 = 0.0211\left[(0.667\ \emptyset_{PL} J)^{\frac{1}{6}}\right]$$

Furthermore, the FRET rate can be calculated by the following equation[3]

$$K_{FRET} = \frac{1}{\tau}\left[(\frac{r_0}{r_{DA}})^6\right]$$

Where τ is the lifetime of donor which can be fitted from TA kinetics of donor (see Figure S3), r_{DA} is the nearest distance of the adjacent molecular between donor and NFAs. The value of $\emptyset_{PL}, J$, r_0, τ, r_{DA} and

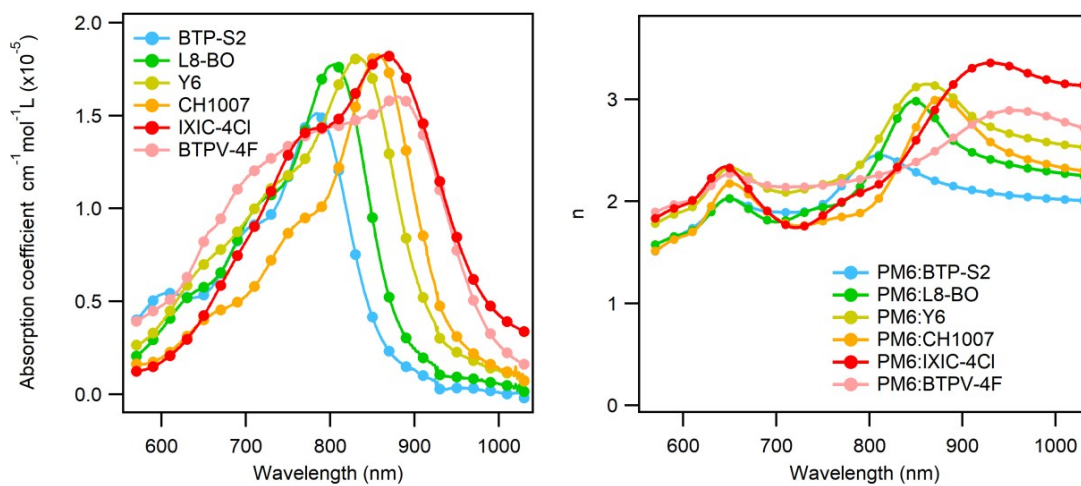K_{FRET} were summarized in Table S2.

Figure S11. Absorption coefficient of neat NFAs films (left) and the refractive index (n) of PM6: NFAs films (right).

Table S2. Detail parameters of Förster Resonance Energy Transfer (FRET) radius (r_0), FRET rate (K_{FRET}) and FRET efficiency (η_{FRET}).

Sample	$\emptyset_{PL}$ (%)[a]	J	r_0 (nm)	τ (ps)[b]	$K_{FRET}^{r_{DA}(1\,nm)}$ (s^{-1})[d]	η_{FRET} (%)	η_{ET} (%)	f
PM6:BTP-S2	1.26	$1.43*10^{15}$	3.19	106	$1.00*10^{13}$	30.3	69.7	0.43
PM6:L8-BO	1.26	$1.78*10^{15}$	3.31	106	$1.25*10^{13}$	61.1	38.9	1.57
PM6:Y6	1.26	$1.18*10^{15}$	3.09	106	$8.21*10^{12}$	47.3	52.7	0.90
PM6:CH1007	1.26	$1.76*10^{15}$	3.30	106	$1.23*10^{13}$	50.6	49.4	1.02
PM6:IXIC-4Cl	1.26	$2.09*10^{15}$	3.40	106	$1.46*10^{13}$	65.9	34.1	1.93
PM6:BTPV-4F	1.26	$1.90*10^{15}$	3.35	106	$1.33*10^{13}$	58.5	41.5	1.41

a. $\emptyset_{PL}$ was acquired from the literature reported.[5]

b. τ was fitted from the TA kinetics of neat PM6 film shown in Figure S3.

c. r_{DA} (0.39 nm) was determined according to the results of simulation calculation.[6]

d. r_{DA} (1nm) was assumed according to the similar assumption from the literature.[5]

e. η_{ET} (%) was calculated according to the approximate formula $\eta_{FRET} + \eta_{ET} = 1$, as the >0.3 eV PM6/NFAs LUMO offsets providing sufficient ET driving force.

f. f was the fraction of two dissociation pathways (ET&FRET), which equals to η_{FRET}/η_{ET}, if the value of f is over 1, the FRET becomes a more efficient way to dissociate donor excitons than direct ET.

Note S3

The internal quantum efficiency (IQE) was extracted based on the following equation,

$$IQE = \frac{EQE}{L_{ab}}$$

Here, EQE is the external quantum efficiency shown in Figure 4c, L_{ab} is the percent of incident light absorbed by the OSC devices, which estimated based on the following equation,[7]

$$L_{ab} = \chi[\sigma + (1 - \sigma)\varphi]$$

Where σ is the light absorption of the blend films, which can be acquired based on Lambert-Beer Law and the absorbance result shown in Figure S9; φ is the light reflectivity of silver shown in Figure S12a and χ is the light transmittance of ITO shown in Figure S12b.
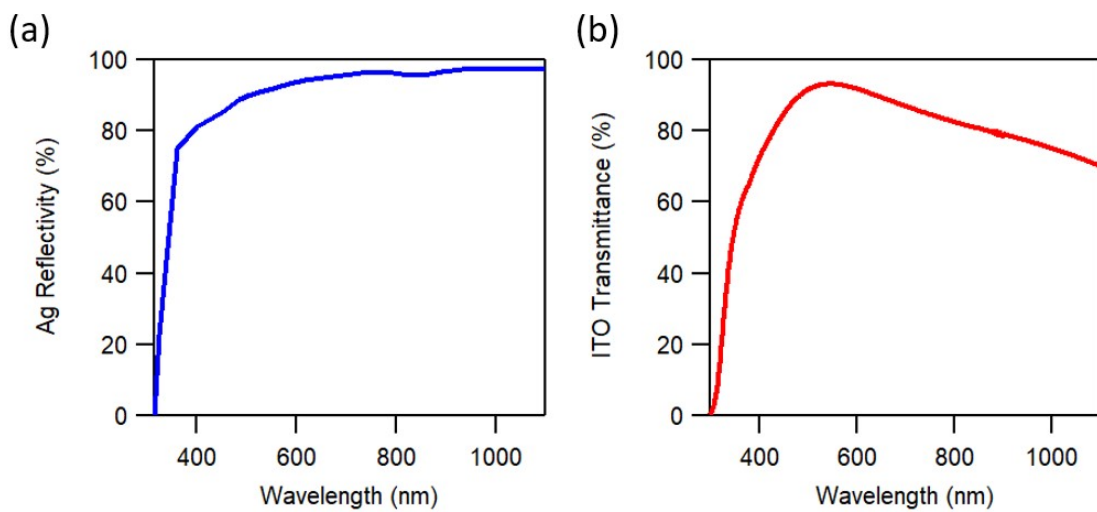

Figure S12. Light reflectivity spectra of silver and light transmittance spectra of ITO.

Table S3. Calculation results of IQE of donor (PM6) and accsptor (NFAs) for different blend films

Sample	Wavelength (nm)[a]	Absorbance	σ (%)	χ	φ	L_{ab}	EQE (%)	IQE (%)
PM6:BTP-S2	620 (D)	0.891	0.871	0.909	0.941	0.888	80.2	90.3
	770 (A)	0.743	0.819	0.837	0.965	0.805	76.6	95.1
PM6:L8-BO	620 (D)	0.811	0.845	0.909	0.941	0.880	85.6	97.2
	800 (A)	0.828	0.851	0.826	0.961	0.804	79.4	98.8
PM6:Y6	620 (D)	0.944	0.886	0.909	0.941	0.892	86.6	97.1
	810 (A)	0.866	0.864	0.821	0.961	0.802	76.2	95.0
PM6:CH1007	620 (D)	0.884	0.869	0.909	0.941	0.887	84.2	94.9
	820 (A)	0.816	0.847	0.818	0.961	0.795	75.9	95.5
PM6:IXIC-4Cl	620 (D)	0.846	0.857	0.909	0.941	0.884	73.4	83.0
	850 (A)	0.736	0.816	0.806	0.96	0.774	63.0	81.4
PM6:BTPV-4F	620 (D)	0.718	0.809	0.909	0.941	0.867	50.8	58.6
	860 (A)	0.539	0.711	0.803	0.96	0.729	40.2	55.1
PM6:PCBM	620 (D)	0.511	0.692	0.909	0.941	0.811	78.1	96.3
	480 (A)	0.560	0.724	0.896	0.882	0.807	78.1	96.8

a. Note that different wavelength can be regarded as the photo-to-charge efficiency of donor/acceptor

Note S4

The details of PM6: PCBM results. Here, only ET occurred after exciting the donor, showing the sufficient driving force (>0.3 eV energy offsets) and the high IQE. However, the large Voc loss and trade-off between Voc and Jsc is apparent.
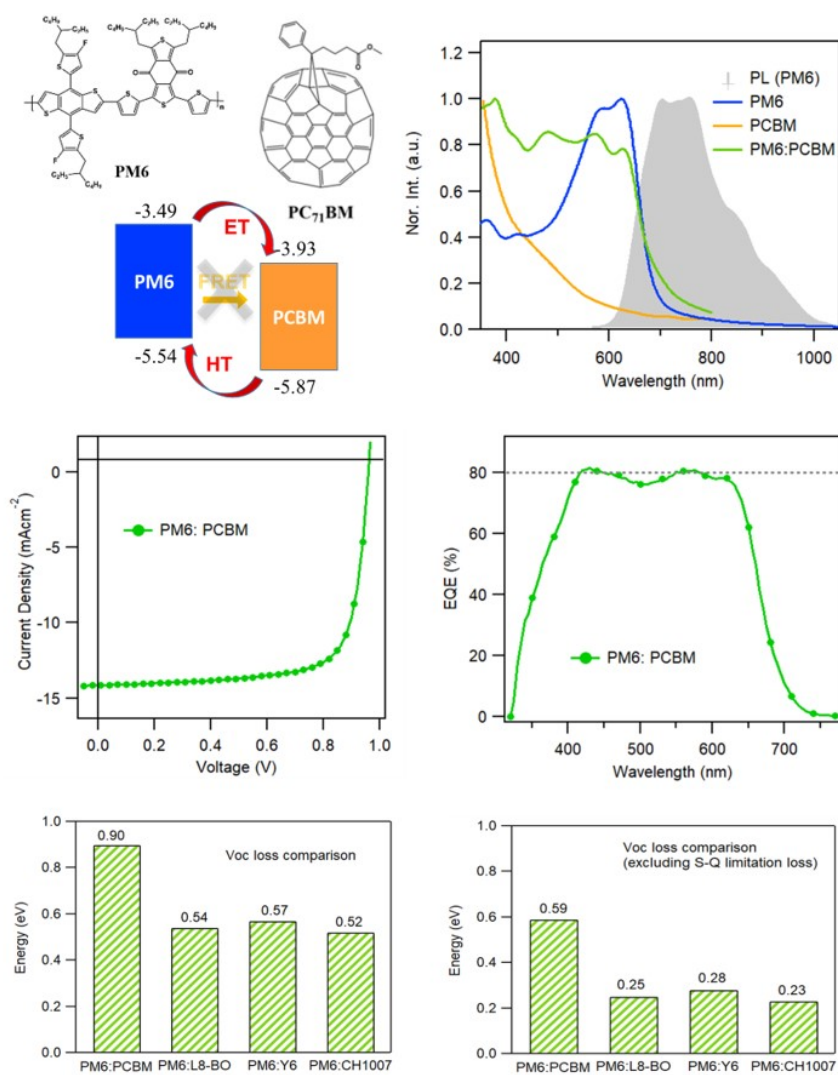

Table S4. Photovoltaic parameters of PM6: PCBM.

OSC	V_{OC} (V)	J_{SC} (mA cm^{-2})	FF (%)	PCE (%)	IQE$_D$ (%)	IQE$_A$ (%)	ΔLUMO (eV)	ΔHOMO (eV)
PM6:PCBM	0.95 (0.95±0.01)	14.29 (14.21±0.12)	74.3 (73.0±1.2)	10.08 (10.01±0.10)	96.3	96.8	0.44	0.33

(a) The average photovoltaic parameters were obtained from 8 devices.

(b) Details of internal quantum efficiency (IQE) calculation were shown in Note S3.

Note S5

The non-radiatived recombination energy loss (ΔV_{nr}) were calculated using the following equation [8]

$\Delta V_{nr} = \Delta E = -kTln(EQE_{EL})$, where k is the Boltzmann constant, T is the temperature. The value of EQE_{EL} and ΔV_{nr} were shown below.

Table S5. Detail parameters of V_{oc}, EQE_{EL} and ΔV_{nr}.

Sample	V_{oc} (V)	EQE_{EL}	ΔV_{nr} (eV)
PM6:BTP-S2	0.95	0.000164	0.23
PM6:L8-BO	0.88	0.000272	0.21
PM6:Y6	0.84	0.000058	0.26
PM6:CH1007	0.83	0.000251	0.21
PM6:IXIC-4Cl	0.76	0.000095	0.24
PM6:BTPV-4F	0.76	0.000590	0.19
PM6:PCBM	0.95	0.000001	0.36

Note S6

Table S6. Details of optimized preparation conditions of BHJ films and neat films.

Sample	D:A	Concentration	Speed/Time	Annealing
PM6:BTP-S2	1:1.2	17.6 mg/mL	3000 rpm/30s	120°C,10min
PM6:L8-BO	1:1.2	16.5 mg/mL	2700 rpm/30s	80°C,10min
PM6:Y6	1:1.2	17.6 mg/mL	3000 rpm/30s	100°C,10min
PM6:CH1007	1:1.2	17.6 mg/mL	3500 rpm/30s	100°C,10min
PM6:IXIC-4Cl	1:1.2	17.6 mg/mL	2000 rpm/30s	90°C,10min
PM6:BTPV-4F	1:1.2	17.6 mg/mL	3000 rpm/30s	100°C,10min
PM6:PCBM	1:1.2	17.6 mg/mL	2000 rpm/30s	100°C,10min
Neat BTP-S2		9.6 mg/mL	3000 rpm/30s	120°C,10min
Neat L8-BO		9 mg/mL	2700 rpm/30s	80°C,10min
Neat Y6		9.6 mg/mL	3000 rpm/30s	100°C,10min
Neat CH1007		9.6 mg/mL	3500 rpm/30s	100°C,10min
Neat IXIC-4Cl		9.6 mg/mL	2000 rpm/30s	90°C,10min
Neat BTPV-4F		9.6 mg/mL	3000 rpm/30s	100°C,10min
Neat PCBM		9.6 mg/mL	2200 rpm/30s	100°C,10min

The total concentration in PM6:BTP-S2, PM6:Y6, PM6:CH1007, PM6:IXIC-4Cl, PM6:BTPV-4F and PM6:PCBM solutions was 17.6 mg/mL and that in PM6:L8-BO was 16.5mg/mL. The weight ratio of

donor and acceptor is 1:1.2 and the fabrication process were listed above, leading to the best device performance.

Reference

[1] Li, S.; Zhan, L.; Jin, Y.; Zhou, G.; Lau, T. K.; Qin, R.; Shi, M.; Li, C. Z.; Zhu, H.; Lu, X.; Zhang, F.; Chen, H. Asymmetric Electron Acceptors for High-Efficiency and Low-Energy-Loss Organic Photovoltaics. *Adv. Mater*. **2020**, 2001160.

[2] Jia, Z.; Qin, S.; Meng, L.; Ma, Q.; Angunawela, I.; Zhang, J.; Li, X.; He, Y.; Lai, W.; Li, N.; Ade, H.; Brabec, C.; Li, Y. High performance tandem organic solar cells via a strongly infrared-absorbing narrow bandgap acceptor. *Nat. Commun.* **2021**, 12, 178.

[3] Jeon, W. S.; Park, T. J.; Kim, S. Y.; Pode, R.; Jang, J.; Kwon, J. H. Ideal Host and Guest System in Phosphorescent OLEDs. *Org. Electron.* **2009**, 10, 240– 246.

[4] Kerremans, R.; Kaiser, C.; Li, W.; Zarrabi, N.; Meredith, P.; Armin, A. The Optical Constants of Solution-Processed Semiconductors—New Challenges with Perovskites and Non-Fullerene Acceptors. *Adv. Optical Mater.* **2020**, 8 (16), 2000319.

[5] Karuthedath, S.; Gorenflot, J.; Firdaus, Y.; Chaturvedi, N.; De Castro, C. S. P.; Harrison, G. T.; Khan, J. I.; Markina, A.; Balawi, A. H.; Pena, T. A. D.; Liu, W.; Liang, R. Z.; Sharma, A.; Paleti, S. H. K.; Zhang, W.; Lin, Y.; Alarousu, E.; Anjum, D. H.; Beaujuge, P. M.; De Wolf, S.; McCulloch, I.; Anthopoulos, T. D.; Baran, D.; Andrienko, D.; Laquai, F. Intrinsic efficiency limits in low-bandgap non-fullerene acceptor organic solar cells. *Nat. Mater.* **2021**, 20, 378– 384.

[6] Han, G.; Guo, Y.; Ma, X.; Yi, Y. Atomistic Insight into Donor/Acceptor Interfaces in High-Efficiency Nonfullerene Organic Solar Cells. *Solar RRL* **2018**, 2, 1800190.

[7] Chen, Z.; Chen, X.; Qiu, B.; Zhou, G.; Jia, Z.; Tao, W.; Li, Y.; Yang, Y. M.; Zhu, H. Ultrafast Hole

Transfer and Carrier Transport Controlled by Nanoscale-Phase Morphology in Nonfullerene Organic Solar Cells. *J. Phys. Chem. Lett.* **2020**, 11 (9), 3226– 3233.

[8] Chen, Z.; Chen, X.; Jia, Z.; Zhou, G.; Xu, J.; Wu, Y.; Xia, X.; Li, X.; Zhang, X.; Deng, C.; Zhang, Y.; Lu, X.; Liu, W.; Zhang, C.; Yang, Y.; Zhu, H., Triplet exciton formation for non-radiative voltage loss in high-efficiency nonfullerene organic solar cells. *Joule* **2021**, 5, 1832-1844.